Astronomy & Astrophysics manuscript no. output
April 27, 2024

Methyl Acetylene Population Diagrams for S140 and TMC-1

Abad Martín, Ángela[1]

Astronomy department, Stockholm University, Roslagstullsbacken 21, 114 21 Stockholm
e-mail: angela.abad2000@gmail.com

April 27, 2024

ABSTRACT

Aims. To deduce the kinetic temperature of the cold and dense molecular clouds S140 and TMC-1, as well as the total column density of their methyl acetylene molecule utilizing radio analysis conducted at the Onsala Space Observatory.
Methods. Spectral emission lines of the K-multiplet from the rotational transition $J = 6 \rightarrow 5$ are detected, under the assumption of local thermodynamic equilibrium (LTE), through the use of a data reduction software (XS). Through this analysis, population diagrams can be generated, allowing us to estimate the desired parameters.
Results. S140 temperature estimate lies in the interval $T_{S140} = (34.72 \pm 2.75)\ K$ and its molecular column density ranges in $N_{S140} = (2.83 \pm 0.38) \cdot 10^{14}\ cm^{-2}$; whereas for TMC-1 we arrived to $T_{TMC-1} = (36.98 \pm 12.43)\ K$ and $N_{TMC-1} = (1.15 \pm 0.62) \cdot 10^{14}\ cm^{-2}$.
Conclusions. Although the population diagram can be considered a highly effective tool for deducing physical conditions within dense clouds when applied to accurately collected and integrated data, as in the case of S140, it can lead to less reliable results when applied to poorly obtained signals, failing to provide meaningful insights, as occured with TMC-1. Nevertheless, these results could provide valuable guidance for future studies, giving background comparison in an attempt to perfection the observation mechanism and giving a new perspective into the study of star-forming regions.

Key words. methyl acetylene (CH_3C_2H) — population diagram — molecular clouds: S140, TMC-1 — LTE

1. Introduction

The study of star-forming regions has consistently occupied a central position in the field of astronomy, continuously offering fresh insights into the formation and evolution processes regarding these sources. It occurs primarily within the interstellar medium (ISM), particularly in regions where dense clouds with low temperatures facilitate the formation of molecules (Hansen (2024b)). These can collide with one another, undergoing transitions between different rotational energy levels (with angular momentum J) (Hansen (2024b)), and can be observed using microwave and far-infrared spectroscopy (McHale (2017)). The examination of these signals provides information about the properties of the molecules and, thus, about the gas and the cloud conditions.

According to studies like that of Kuiper *et al.* (1984), methyl acetylene (CH_3C_2H) proves to be a convenient molecule for this purpose, being a dependable tool for assessing kinetic temperatures within dense molecular clouds. Knowing that the projection of J along the symmetry axis of the molecule is quantized via the K-parameter, we can associate K-multiplets to J transitions and establish a relationship between the K-ladders population and the collisional excitation of the molecules (Hansen (2024a)). Based on Kuiper *et al.* (1984) findings, the conditions of the clouds under investigation in this project (S140 and TMC-1) adequately sustain reasonable population levels at the J=6 level. Consequently, we focus on the characterization of the K-multiplet ($K = 0, 1, 2, 3$) emission lines obtained as a result of the transition from the upper ($J_u = 6$) to the lower angular momentum level ($J_l = 5$).

This way, employing radio techniques with the use of the 20m telescope at the Onsala Space Observatory (OSO) in Gothenburg, Sweden (Johansson *et al.* (2016)), we can determine the spectra for both sources in an attempt to characterize the multiplet emission lines and, using a technique called "population diagram" (see Section 3), derive the corresponding temperature for each cloud, as well as their molecular column densities.

2. Observations

The planning for visiting the OSO was established between April 10th and April 12th, scheduling the observations from the afternoon of April 11th till the afternoon of April 12th. However, because of the onset of rain, the observations concluded around noon on the 12th. Additionally, the organization for observing each object was individually decided upon their peak visibility, with the observing plan set so as to track them when their altitude was ≈30 ° or higher (airmass.org (2024) was used to determine the visibility plots). This way, we could detect S140 two times during the same day (in the afternoon (obs. 1) and during the night (obs. 2)) whereas TMC-1 was only measured right before nighttime while it was setting (see Table 1).

The observations started by initially selecting SiO maser sources (AGB stars), which were used as calibration stars for performing what is known as *spectral line pointing*. This is a technique that is used to uphold an accuracy of 3" rms in both azimuth and elevation (Johansson *et al.* (2016)). Also, *focusing* was applied, based on rearrangements of the mirrors and subreflectors so as to obtain a better signal. The former had to be measured before every science observation whereas the latter could be calibrated every couple of hours. After that, and taking care of changing the molecule to our desired one (CH_3C_2H), we could start measuring the science sources.

	Sources	
Parameters	**S140**	**TMC-1**
α [h:min:s]	22:54:41.20	04:41:45.90
δ [°:':"]	+63:03:43.00	+25:41:26.99
t_{obs} [h:min]	12:24 UT (obs. 1) 21:16 UT (obs. 2)	15:43 UT
$t_{exp}/file$ [s]	240	240
Humidity [%]	94.30 (obs. 1) 92.90 (obs. 2)	86.20
T_{sys}^{in} [K]	357.4 – 359.8 (obs. 1) 276.6 – 275 (obs. 2)	195.4 – 195.7
T_{sys}^{end} [K]	no data (obs. 1) 471.3 – 470.2 (obs. 2)	348.5 – 350.1

Table 1: S140 and TMC-1 parameters retrieved from Hansen (2024c) and Hansen *et al.* (2024). The following is shown: right ascension (α), declination (δ), starting time of the observation (t_{obs}), exposure time (t_{exp}) per file, humidity and system temperatures (T_{sys}) before and after the measurements (Olberg (2024)).

3. Analysis

Following the acquisition of multiple raw files from the observation procedure outlined in Section 2 (35 *.fit* files in total for S140 and 20 for TMC-1), the subsequent step involved the reduction of data for each source. This process required the implementation of two tools: `XS` software (developed by Per Bergman at OSO, (Johansson *et al.* (2016))) for primary data reduction and `Python` as the programming language to calculate the corresponding parameters using what is known as the population diagram method.

3.1. XS data reduction

The reduction process started by selecting the corresponding raw files for each source and selecting the option *Open Sequence* so as to visualize them in a "map" mode. Next step consisted on using the reduction tool to average all the scans in order to obtain one single *.fit* file per source. This averaging was executed by using the *System temp. and Int. time* option, meaning that the combination of the images took into account the system temperature as well as the integration time required while detecting each file (see Table 1).

Afterwards, it was necessary to enhance the Signal-to-Noise Ratio (SNR) to acquire more precise data while minimizing noise interference and that was achieved by *Redressing* the spectra, that is, reducing the spectral resolution. The following step consisted on aligning the spectrum with respect to the zero baseline, which helped remove biases as well as facilitating the interpretation of results, thereby increasing their precision. To do so, we started by generating two baseline boxes on each side of the spectrum, trying to cover as much area as possible without selecting the emission-line region, and then fitted and subtracted a first degree polynomial to linearize the spectra.

At this moment, the spectra for both sources were completely reduced and we could start analyzing the spectral lines. We started by fitting Gaussian profiles to each signal in an attempt to characterize them and obtain their associated frequencies (see Fig. 1). These experimental values were compared to the tabulated frequencies proposed in Table 1 of Hansen (2024a), which helped us classify the emission lines with their corresponding K-multiplet.

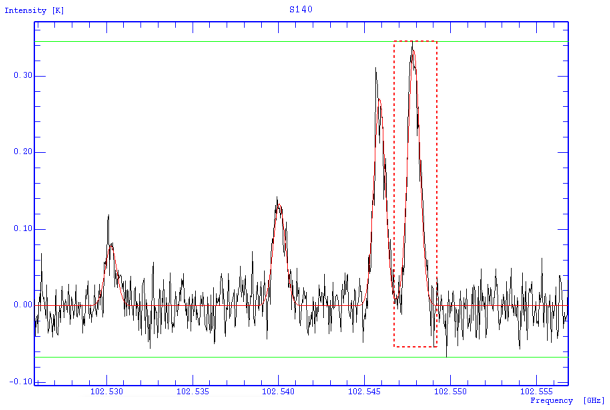

(a) S140

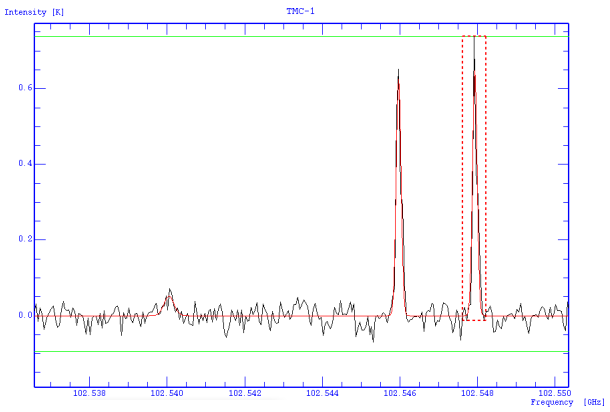

(b) TMC-1

Fig. 1: Representation of the reduced spectra for the different clouds using `XS` software. Gaussian fitting has been applied (solid red curves), as well as the detection of the integrated intensities through the use of moment boxes (an example is shown as a dashed red box). (a) S140 shows the four multiplet emission lines going from K=3 to K=0 reading from left to right. (b) TMC-1 shows three out of the four multiplet emission lines (mainly due to a decrees in data quality) from K=2 to K=0 reading from left to right.

The categorization was established from K=3 to K=0 reading the spectra from left to right and we applied the tabulated results during the data analysis for accuracy purposes. Additionally, it is worth commenting on the inadequate data quality of TMC-1, confirmed by the inability to detect the line associated to K=3.

The last step before proceeding with the population diagram technique consisted on fitting moment baselines to the Gaussian profiles. This ensured the measurement of the integrated intensities for each signal (see Table 2 and Fig. 1 for an example).

	I [K·km/s]	
K-multiplets	**S140**	**TMC-1**
K=3	0.197 ± 0.033	no data
K=2	0.326 ± 0.032	0.0515 ± 0.0181
K=1	0.645 ± 0.035	0.290 ± 0.019
K=0	0.847 ± 0.038	0.296 ± 0.017

Table 2: Experimental values for the integrated intensities retrieved from the moment-baseline fitting performed with `XS`.

3.2. Population Diagram

Once the data was properly reduced and the K-multiplet emission lines were correctly classified and parameterized, we initiated the procedure to develop what is known as the population diagram.

This technique, which is based on the characterization of cloud properties from their molecular rotational transitions in the form of emission lines, is defined, according to Goldsmith *et al.* (1999) as the "plot of the column density per statistical weight of a number of molecular energy levels as a function of their energy above the ground state". And that is precisely what is described in the following procedure, which has been principally retrieved from the instructions given by Hansen (2024a).

On the one hand we have that the column density of the upper state for an optically thin transition is given by

$$N_u = \frac{8\pi k_B \nu^2}{hc^3 A_{ul} \eta_{mb}} \cdot \int T_A d\nu \equiv \frac{8\pi k_B \nu^2}{hc^3 A_{ul} \eta_{mb}} \cdot I \tag{1}$$

in mks units, where $\int T_A d\nu \equiv I$ is the integrated antenna temperature ("the brightness temperature averaged across the antenna beam weighted with the normalized power pattern" (Olberg (2024))) which is given by the integrated intensity of the transitions (estimated with the fitting of moment boxes, see Section 3.1), A_{ul} is the Einstein coefficient for spontaneous emission for each line and η_{mb} refers to the main beam efficiency of the telescope (≈ 0.5). In order to compute Eq. (1) per emission line, the tabulated values for ν were introduced, as well as the integrated intensities computed with `XS` (see Table 2). Additionally, the following expression was applied for the Einstein coefficients

$$A_{ul} \approx 1.165 \cdot 10^{-11} \nu^3 \mu^2 \frac{J_u^2 - K^2}{J_u(2J_u + 1)} \tag{2}$$

where μ is the dipole moment (0.75 Debye) and J_u is the angular momentum of the upper state (which, let's remember, was $J_u = 6$). To get a coherent result in terms of dimensions while using Eq. 2, it was important to introduce the frequencies in $[GHz]$.

On the other hand, and assuming a Local Thermodynamic Equilibrium (LTE) for our problem (transitions sharing the same excitation temperature), we know from the Boltzmann equation that the population for the upper level in each line is given by

$$N_u = \frac{N}{Z} \cdot g_u \cdot e^{-\frac{E_u}{k_B \cdot T}} \Rightarrow ln\left(\frac{N_u}{g_u}\right) = -\frac{1}{T} \cdot \frac{E_u}{k_B} + ln\left(\frac{N}{Z}\right) \tag{3}$$

with N being the total column density of the molecule $[m^{-2}]$, Z representing the partition function (usually approximated by $Z \approx 0.523 \cdot T^{3/2}$ [dim.less.]), g_u being the statistical weight of the upper level [dim.less.] (see Hansen (2024a)) and E_u representing the energy above the ground for each transition (given by Table 1 in Hansen (2024a)). The second term in Eq. 3 can be easily compared to a first-degree equation $y = m \cdot x + b$, with slope $m = \frac{-1}{T}$ and intercept $b = ln\left(\frac{N}{Z}\right)$. This way, by representing the column density per statistical weight for each emission line as a function of their energy above the ground state (normalized by the Boltzmann's constant), we could obtain the population diagram from which we could easily estimate both the temperature as well as the molecule's column density by adjusting through a linear fitting.

4. Results

Applying the former mathematical procedure to our science frames and using `Python` techniques when fitting linear regressions to our experimental data, we obtained the final results shown in Fig. 2 and Table 3. On the one hand, it is important to mention that after a deep analysis trying to determine the best linear-fitting mechanism to apply to the data, we decided to use *scipy.optimize.curve_fit* from `Python` (Jones *et al.* (2001)) since it was the best option as it considered the error bars associated to the individual data-points when determining the errors for the slope and the intercept, giving more accurate results. On the other hand, it is worth noting the different expressions applied when calculating the rest of the uncertainties associated with the desired parameters, all of them derived through propagation methods as follow:

$$\delta\left(ln\left(\frac{N_u}{g_u}\right)\right) = \left|\frac{1}{I}\right| \delta I \tag{4}$$

$$\delta T = \left|\frac{1}{m^2}\right| \delta m \tag{5}$$

$$\delta N = \sqrt{\left(\left|0.523 \frac{3}{2} T^{1/2} e^b\right| \delta T\right)^2 + \left(\left|0.523 T^{3/2} e^b\right| \delta b\right)^2} \tag{6}$$

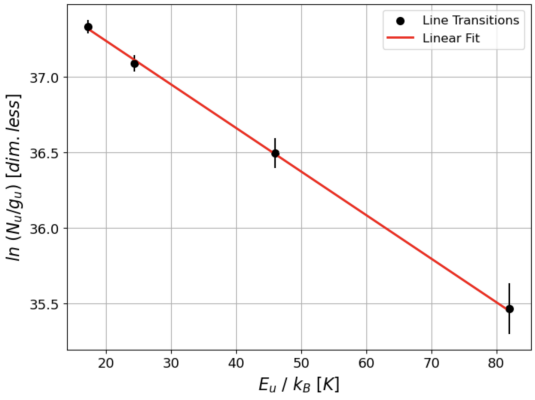

(a) S140

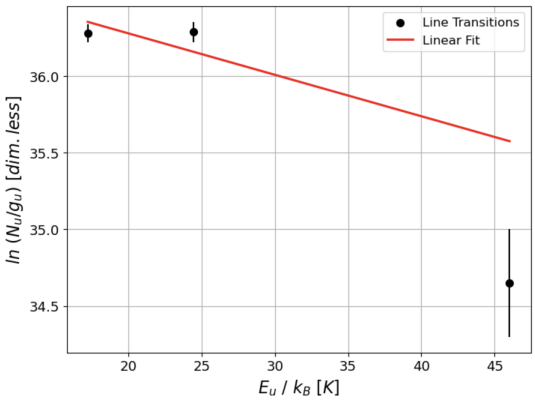

(b) TMC-1

Fig. 2: Population diagrams for the K-multiplets associated with the molecular rotational transition $J = 6 \rightarrow 5$. (a) S140 and (b) TMC-1.

	Sources	
Results	**S140**	**TMC-1**
m [K^{-1}]	-0.029 ± 0.002	-0.027 ± 0.009
b [dim.less.]	37.82 ± 0.07	36.82 ± 0.19
T [K]	34.72 ± 2.75	36.98 ± 12.43
N [cm^{-2}]	$(2.83 \pm 0.38)\cdot 10^{14}$	$(1.15 \pm 0.62)\cdot 10^{14}$

Table 3: Final results for S140 and TMC-1 retrieved from personal `Python` code.

5. Discussion

When comparing S140's results (see Table 3) with those stated in Table 3 of Alakoz *et al.* (2002) (T=(26 ± 1) K and N=(2.8 ± 0.2)·$10^{14} cm^{-2}$) we observe that despite the temperatures not matching completely (although being of roughly the same order), the density values are perfectly aligned, suggesting possible differences in the way of treating the data (for instance, their values for the integrated intensities differ from ours particularly in the multiplets K=1 and 0, see Table 2 in Alakoz *et al.* (2002)). On the other hand, studies like that of Kuiper *et al.* (1984) show temperatures of the order of (32.1 ± 6.7)K, contributing to the idea that our final results for S140 lie among the expected for similar observational procedures.

However, upon examining TMC-1 (see Table 3), the situation shifts. According to Kuiper *et al.* (1984), where they estimated the temperature and column density of the cloud in two regions, they obtained mean apparent values of the order of T=(21.7 ± 4.8) K and N=(3.7 ± 0.7)·$10^{13} cm^{-2}$. When comparing these to the ones obtained from our analysis it is easy to perceive that ours lack precision. Not only are the error bars excessively wide for our experimental data (especially for the temperature) but they were obtained from lower quality observational frames (remember that the K=3 line was not resolved), which contributes to the inaccuracy of the results. Nevertheless, general discrepancies could exists since our measurements were taken for the core of the source (also for S140).

Other factors are to be accounted for, such as the observational conditions while obtaining the data. Despite starting the observations with favorable weather, the high values for the humidity could have affected the measurements, as well as the increase of the system temperature (T_{sys}) after each observation, introducing biases and noise to the spectra (see Table 1). Furthermore, TMC-1 was observed just once while setting. This means that during its analysis, not only couldn't a set of images from different observation moments be used (which would have helped with the statistics), but also by being detected while setting, the availability of the source in the sky was reduced, decreasing the quality of the spectrum while increasing the noise. These circumstances did not happen for S140, which could explain why its results are more accurate.

Additionally, it has been observed that after what appears to be a convenient image reduction, the fitting of Gaussian profiles into the emission lines, as well as the selection of moment baselines for the acquisition of the integrated intensities and their errors, rely purely on visual and manual uncertainties based on how precisely you make adjustments with the mouse. This means that for the same corrected image, the final numerical values vary considerably in different measurement attempts. Indeed, for low-resolution lines where higher errors would be anticipated, `XS` provides relatively low values, indicating a lack of accuracy in its computation method.

Finally, it is worth mentioning that the comparison of our data with previous literature in the field is merely done as a guiding-technique, since they tend to follow slightly different analysis with diverse focuses. As a result, these comparisons mainly enable us to broadly assess the consistency of our methods and identify any potential mistakes to be addressed during the procedure.

6. Summary

The study investigates the temperatures and molecular column densities for two cold and dense molecular clouds, S140 and TMC-1, through the implementation of radio astronomy techniques at the Onsala Space Observatory, focusing on the methyl acetylene (CH_3C_2H) molecule as a diagnostic tool. Following the observation planning detailed in Section 2 and the computational procedure detailed in Section 3, with the assistance of tools such as the `XS` software or `Python`, the corresponding analysis was conducted giving population diagrams as an output (see Table 3 for the results).

The study encountered challenges, particularly with the quality of the TMC-1 data, which affected the reliability of the results. While S140 yielded remarkably precise estimates aligning with literature values, TMC-1's measurements exhibited wider error margins, suggesting potential biases introduced during the observation and data reduction processes with `XS`, principally.

Overall, the study highlights the effectiveness of radio analysis and population diagram techniques in characterizing molecular clouds and provides insights for future research in star-forming regions.

Acknowledgements. We sincerely thank the Onsala Space Observatory for enabling our initiation into radio astronomy, fostering our scientific development and autonomy in data analysis. We also extend our gratitude to Terese Thidemann and Anamaria Gkini for their exceptional guidance and support.

References

Alakoz, A. V., Kalenskii, S. V., Promislov, V. G., Johansson, L. E., & Winnberg, A. (2002). Parameters of warm molecular clouds from methyl acetylene observations. Astronomy Reports, 46, 551-566.

arimass.org. (2024). Visibility Plot. (`https://airmass.org/chart/obsid:onsala/date:2024-04-11/object:S140/ra:343.671667/dec:63.061944/object:TMC-1/ra:70.441250/dec:25.690831`).

Goldsmith, P. F., & Langer, W. D. (1999). Population diagram analysis of molecular line emission. The Astrophysical Journal, 517(1), 209.

Hansen, T. T. (2024). Methyl Acetylene (CH_3C_2H) as a Temperature Probe. Athena (`https://athena.itslearning.com/`), Observational Astrophysics II, Stockholm University, Sweden.

Hansen T. T. (2024). Lecture 1. Athena (`https://athena.itslearning.com/`), Observational Astrophysics II, Stockholm University, Sweden.

Hansen T. T. (2024). Lecture 2. Athena (`https://athena.itslearning.com/`), Observational Astrophysics II, Stockholm University, Sweden.

Hansen T. T. & students (2024). ObsSchedule2024.xlsx. Athena (`https://athena.itslearning.com/`), Observational Astrophysics II, Stockholm University, Sweden.

Johansson, L. E., Olofsson, A., & Beck, E. D. (2016). OSO 20 m Telescope Handbook. Onsala Space Observatory, Report. Athena (`https://athena.itslearning.com/`), Observational Astrophysics II, Stockholm University, Sweden.

Jones, E., Oliphant, T., Peterson, P., et al. (2001). SciPy: Open Source Scientific Tools for Python. (`http://www.scipy.org/`).

Kuiper, T. B. H., Kuiper, E. R., Dickinson, D. F., Turner, B. E., & Zuckerman, B. (1984). Methyl acetylene as a temperature probe for dense interstellar clouds. Astrophysical Journal, Part 1 (ISSN 0004-637X), vol. 276, Jan. 1, 1984, p. 211-220. NASA-supported research., 276, 211-220.

McHale, J. L. (2017). Molecular spectroscopy, Second Edition. CRC Press.

Olberg, M. (2024). Introduction to Radio Astronomy. Chalmers University of Technology (Department of SPACE, EARTH and ENVIRONMENT). Athena (`https://athena.itslearning.com/`), Observational Astrophysics II, Stockholm University, Sweden.